

# Electronic Supplementary Information:

## Acoustic bubble dynamics in a yield-stress fluid

Brice Saint-Michel\* and Valeria Garbin\*<sup>‡</sup>

### 1 Uncertainties on the thermal and acoustic damping parameters

The uncertainties for the basic quantities involved in dissipation (medium density  $\rho$ , initial bubble radius  $R_0$ , acoustic frequency  $f$ , sound velocity  $c$ , ambient pressure  $p_0$ ) have been estimated from our measurements:

$$\begin{aligned} \left| \frac{\delta\rho}{\rho} \right| &\simeq 5 \times 10^{-3} & \left| \frac{\delta R_0}{R_0} \right| &\simeq 5 \times 10^{-3} \\ \left| \frac{\delta f}{f} \right| &\leq 1 \times 10^{-3} & \left| \frac{\delta c}{c} \right| &\simeq 5 \times 10^{-3} \\ \left| \frac{\delta p_0}{p_0} \right| &\simeq 5 \times 10^{-3} & & \end{aligned}$$

The uncertainty regarding thermal diffusion has been estimated from different sources [Refs. (25) and (39)] to be around:

$$\left| \frac{\delta D}{D} \right| \simeq 0.05 \quad (1)$$

We have then:

$$\left| \frac{\delta \text{Pe}}{\text{Pe}} \right| \simeq 0.06$$

At this specific Péclet number, the uncertainty on the thermal diffusion index  $\kappa'$  reads

$$\left| \frac{\delta \kappa'}{\kappa'} \right| \simeq 0.02$$

The major source of uncertainty in  $\eta_{\text{th}}$  then comes from that of  $\kappa'$ , leading to an uncertainty on the overall  $\eta$  that we can estimate from Figure 9 (from the Appendix):

$$|\delta\eta_{\text{th}}| \simeq \eta_{\text{th}} \left| \frac{\delta\kappa'}{\kappa'} \right| \simeq 50\eta_0 \times 0.02 \simeq \eta_0$$

The uncertainty on  $\eta_{\text{th}}$  is then comparable to the solvent viscosity and to uncertainty related to our fitting procedure. They should then be included in our experimental estimate. Regarding acoustic dissipation, we obtain:

$$\left| \frac{\delta\eta_{\text{ac}}}{\eta_{\text{ac}}} \right| = \left| \frac{\delta c}{c} \right| + 3 \left| \frac{\delta R_0}{R_0} \right| + 2 \left| \frac{\delta f}{f} \right| + \left| \frac{\delta c}{c} \right| \simeq 0.02$$

Based on Figure 9, the overall uncertainty  $|\delta\eta_{\text{ac}}|$  is small compared to the solvent viscosity, mainly because  $\eta_{\text{ac}} \sim \eta_0 \ll \eta_{\text{th}}$ . Acoustic damping can then be safely be neglected in our estimations.

## 2 Bubble dissolution dynamics

Figure SI 1 shows that the bubbles we are working with progressively dissolve in the Carbopol. The dissolving rate varies dramatically between different Carbopol batches. We attribute this fact to the different time the fluid spends in the vacuum chamber before the acquisitions, which itself depends on the amount and the size of the bubbles introduced during the mixing step. In particular, while the Carbopol of Panel (a) has spent more than an hour in the vacuum chamber, the Carbopol of Panel (b) was free of any bubbles following mixing and did not necessitate degassing. We believe that some Carbopol batches are slightly under-saturated with air when starting experiments, which strongly accelerates bubble dissolution<sup>1</sup>.

The impact of the Carbopol yield stress on bubble dissolution is not very well known at the moment: modelling effort has rather worked on the simpler cases of ideal bulk or surface elasticity. Recent experimental results have shown that bubble dissolution can be arrested in attractive yield-stress fluids<sup>2</sup> but the mechanism at play remains unclear.

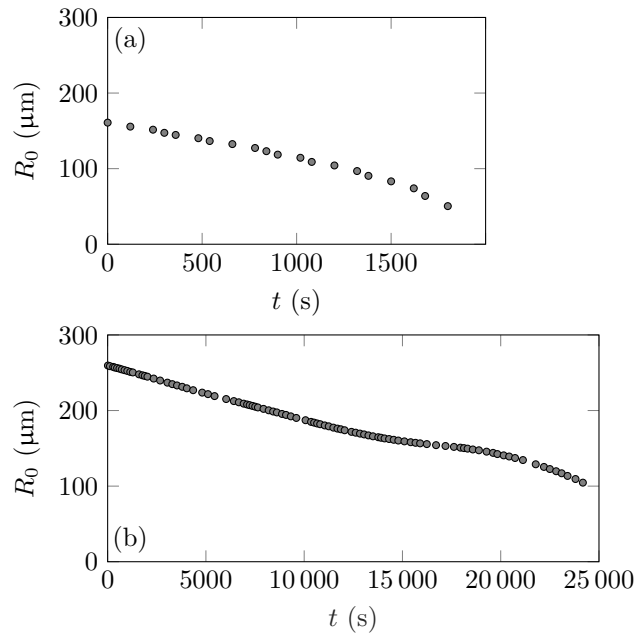


**Fig. SI 1** Evolution of the bubble radius at rest  $R_0$  as a function of time for two bubbles corresponding to two separate Carbopol preparations. Note the different  $x$  axis scales for Panels (a) and (b).

### 3 Impact of oscillatory yield criterion on bubble mobility

We examine in Figure SI 2 the impact of yielding according to the simple yielding criterion  $\zeta \geq 0.043$  [derived from Equation (10)] on the bubble displacement due to Bjerknes forces at location ② of Section 4.3. The interaction between the two phenomena were dismissed in Section 4.3 since recovery was always close to 100%, however we can verify it more thoroughly by re-plotting the data of Figure 4(c) and highlight whether experiments inducing yielding due to oscillations soften the yield-stress fluid and allow larger bubble displacement.

Figure SI 2(a) shows that the oscillation amplitude for the various initial bubble radii  $R_0$  are randomly scattered on the vertical axis: we have indeed applied a broad range of acoustic pressures on such bubbles. We separate the experimental data into two categories, depending on whether they satisfy the oscillatory yielding criterion. We then plot the data from the two categories in Figure SI 2(b)-(c) using different markers. We note a good superposition of the “yielded” and “unyielded” data, confirming that satisfying the yielding criterion for oscillations does neither affect the linear response of the material to Bjerknes forces nor the near-complete recovery after the oscillations have ended.

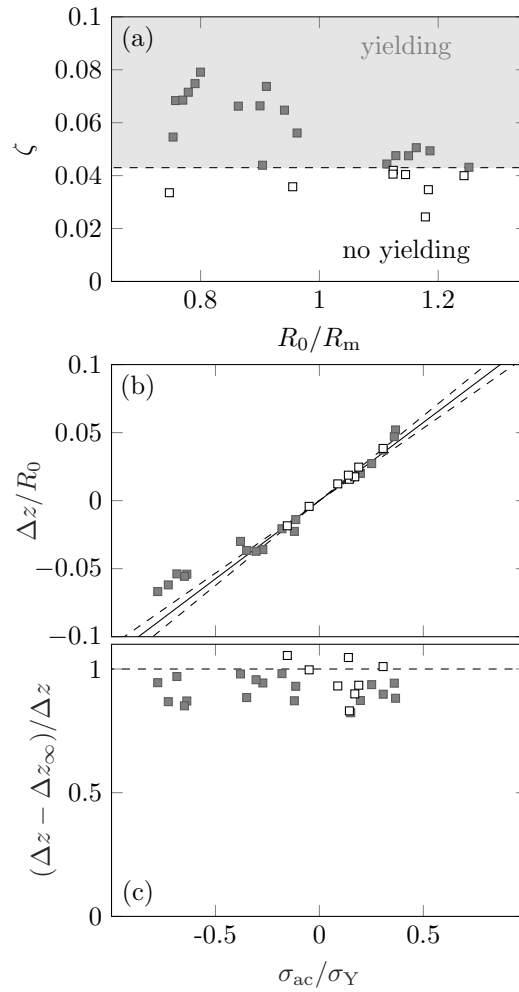


**Fig. SI 2** Influence of the oscillatory yielding criterion  $\zeta \geq 0.043$  on the bubble mobility under acoustic radiation forces. (a) Amplitude of the oscillations  $\zeta$  corresponding to the experiments reported in Figure 4. Markers are formatted according to whether they satisfy  $\zeta \geq 0.043$  which characterises the onset of yielding due to oscillations. (b) Typical strain applied by the bubble motion in the vertical direction  $\Delta z/R_0$  as a function of the stress applied to it by acoustic radiation forces, normalised by the yield stress  $\sigma_Y$  of the fluid. We apply the same formatting for the markers as in Panel (a). (c) Normalized displacement recovery  $(\Delta z - \Delta z_\infty)/\Delta z$  as a function of the stress applied to it by acoustic radiation forces, normalised by the yield stress  $\sigma_Y$  of the fluid. We apply the same formatting for the markers as in Panel (a).

## 4 Influence of residual stresses on bubble shape oscillations

We have examined carefully the shape of one bubble (named bubble (i) in the new version of Figure 6) for five successive acquisitions. The same acoustic excitation is applied from  $ft = 0$  to  $ft = 200$  for the five acquisitions, while the initial radius  $R_0$  progressively decreases due to bubble dissolution. The second acquisition corresponds to the first onset of bubble shape oscillations. Residual stresses may :

1. Provide an initial asymmetry that actually grows for all experiments, yet has not been detected in our data processing, resulting in improper classification as “spherical oscillations”,
2. Impose the shape mode number  $k$  to follow residual stress symmetry,
3. Orient the shape mode nodes and anti-nodes along the main directions of the residual stresses

Figure 3 shows the deviations  $R(\theta, t)/R(t)$  from a spherical shape for these five acquisitions. We may attribute these deviations to residual stresses as they are the only source of asymmetry present in the problem besides gravity; gravity would show as a perturbation with a preferred orientation around  $\theta = \pi/2$  and  $3\pi/2$ .

Before the first onset of shape oscillations, very slight deviations (of order 0.7 %) of the bubble radius are observed, with dipolar  $k = 2$  structure and an orientation roughly compatible with gravity. This first acquisition is very close to the onset of shape oscillations, as the applied pressure is the same as for the second acquisition (where clear shape oscillations are seen) and the initial bubble radius is only 2% larger than in the second acquisition. Yet, no noticeable growth of the deviations from a spherical shape is visible during the oscillations. Hypothesis 1. is therefore unlikely.

In the second acquisition, we clearly observe  $k = 7$  shape modes. Besides not being of the same parity as the initial radial disturbances, the initial orientation of the residual stresses does not correspond to any obvious feature (node, or anti-node) of the shape modes. The shape deviations at the end of the second acquisition, interestingly, still possess a  $k = 2$  symmetry, yet with a different orientation than at the beginning of the acquisition. Further acquisitions show that two successive acquisitions showing the same shape mode number  $k = 7$  (second and third panel) or  $k = 6$  (fourth and fifth panel) do not necessarily have the same orientation (see white dotted line and black dashed line). In addition, successive acquisitions with the same shape mode number lead to different orientations of the shape deviations after the end of oscillations. This is strong evidence that residual stresses (or alternatively, initial shape deviations) can neither impose a shape number  $k$  nor the orientation of shape modes, at variance with Hypotheses 2. and 3.

We could then not observe any direct impact of residual stresses on bubble shape oscillations. However such effects cannot be completely ruled out using this analysis.

### Notes and references

- 1 W. Kloek, T. Van Vliet and M. Meinders, *J. Coll. Interf. Sci.*, 2001, **237**, 158–166.
- 2 S. Saha, B. Saint-Michel, V. Leynes, B. P. Binks and V. Garbin, *Rheol. Acta*, 2020, **59**, 255–266.
- 3 K. Murakami, R. Gaudron and E. Johnsen, *Ultrason. Sonochem.*, 2020, **67**, 105170.
- 4 A. O. Maksimov and T. G. Leighton, *Acta Acust. united Acust.*, 2001, **87**, 322–332.

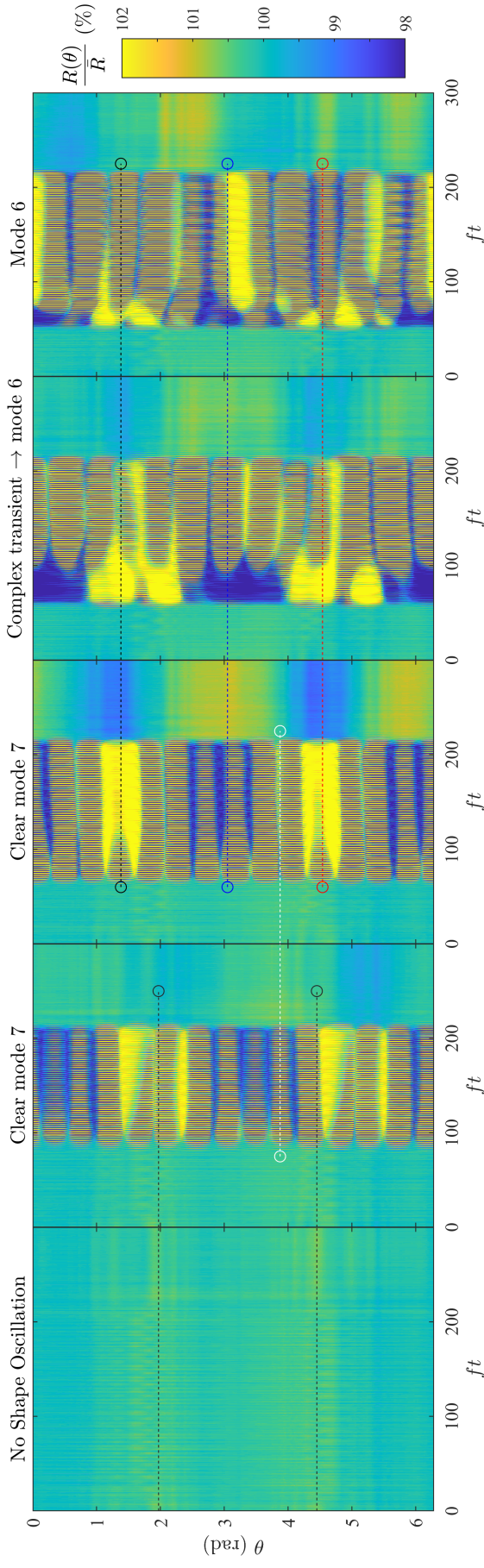


**Fig. S1** 3 Space-time diagram of the non-spherical asymmetries of the bubble for five successive experiments. The acoustic excitation is applied for  $0 \leq ft \leq 200$ . The first experiment does not evidence any shape oscillations: the initial asymmetry (with dipole symmetry) does not increase during the acoustic excitation and its orientation is preserved throughout the acquisition; it is still visible at the beginning of the second panel. During the second acquisition, a clear shape mode  $k = 7$  is established from  $ft \geq 100$  (14 lobes in the vertical direction). The orientation of the shape modes does not specifically follow that of the initial asymmetry, as can be seen from the grey lines, used as visual guides. The shape oscillations rather induce a new dipole asymmetry of the bubble shape once the oscillations have died out. This asymmetry is hardly visible at the beginning of the third acquisition. In addition, while the third experiment also shows a  $k = 7$  shape mode, its orientation differs from that of the previous run (see white dashed line, used as a guide). These shape modes impose a new orientation for the dipole asymmetry after the oscillations have died out. As can be seen from the blue, black and red guide lines, this orientation does not necessarily follow the lobes of the shape modes. The newly-formed dipole orientation seems to be preserved throughout the fourth acquisition, as can be seen before, after, and, to a lesser extent, during the shape oscillations, even though the shape oscillations shift from  $k = 7$  to  $k = 6$ . The dipole orientation is however largely lost after the fifth acquisition; despite showing  $k = 6$  shape modes, their orientation once again differs from the previous run and a new (multipolar ?) residual asymmetry is visible once the oscillations of the fifth run have died out.